A laser-locked cavity ring-down spectrometer employing an analog detection scheme

T. G. Spence, C. C. Harb, B. A. Paldus, and R. N. Zare
Department of Chemistry, Stanford University, Stanford, California 94305

B. Willke and R. L. Byer
Department of Applied Physics, Stanford University, Stanford, California 94305

(Received 25 August 1999; accepted for publication 1 November 1999)

A system is described that employs a diode-pumped Nd:YAG continuous-wave laser source servolocked to a three-mirror optical cavity and an analog detection circuit that extracts the ring-down rate from the exponentially decaying ring-down waveform. This scheme improves on traditional cavity ring-down spectroscopy setups by increasing signal acquisition rates to tens of kilohertz and reducing measurement noise sources. For example, an absorption spectrum of a weak CO_2 transition at 1064 nm is obtained in less than 10 s at a spectral resolution of 75 kHz employing a cavity with an empty-cavity ring-down decay lifetime of 2.8 μs and a total roundtrip path length of 42 cm. The analog detection system enables laser frequency scan rates greater than 500 MHz/s. The long-term sensitivity of this system is $8.8\times10^{-12}\,\mathrm{cm}^{-1}\,\mathrm{Hz}^{-1/2}$ and the short-term sensitivity is $1.0\times10^{-12}\,\mathrm{cm}^{-1}\,\mathrm{Hz}^{-1/2}$. © *2000 American Institute of Physics.* [S0034-6748(00)02602-2]

I. INTRODUCTION

Cavity ring-down spectroscopy (CRDS) is a laser-based absorption technique that can be used to probe concentrations of dilute or weakly absorbing gas-phase species.[1,2] This technique has recently increased in popularity because of its ease of implementation and inherent sensitivity.[3] Indeed, CRDS has been shown to be capable of achieving sensitivities comparable to or exceeding those achieved with photoacoustic and frequency modulation spectroscopies. Unlike these indirect techniques, however, CRDS provides a direct measure of absolute gas-phase concentrations of the absorbing species.

In CRDS, light from a pulsed or continuous-wave (cw) laser source is injected into a high-finesse optical cavity, called the ring-down cavity (RDC), formed by two or more highly reflecting mirrors aligned to form a stable optical resonator. With the input radiation terminated at t_0, the intensity of the light circulating within the optical cavity, I_{circ}, decays exponentially with time, t, as[4]

$$I_{\mathrm{circ}}(t)=I_{\mathrm{circ}}(t_0)\exp\left(\frac{-\delta_c}{T_{\mathrm{rt}}}(t-t_0)\right), \tag{1}$$

where T_{rt} is the roundtrip transit time and δ_c is a measure of the cavity losses, given by

$$\delta_c=\alpha(\lambda)L_{\mathrm{rt}}-\sum_n \ln R_n+A. \tag{2}$$

Here, $\alpha(\lambda)$ is the fraction of light lost to absorbing species within the cavity per cm traveled at wavelength λ, L_{rt} is the roundtrip path length, R_n is the reflectivity of the nth cavity mirror, and A comprises other optical losses including scattering and absorption by the mirror surface. Combining Eqs. (1) and (2), using the simplifying approximations that the mirror reflectivities are all equal, and approximating $\ln(1/R)\approx(1-R)$ for $R\approx1$, we find that the decay of circulating intensity is given by

$$I_{\mathrm{circ}}(t)=I_{\mathrm{circ}}(t_0)\exp\left(\frac{-(\alpha(\lambda)L_{\mathrm{rt}}+n(1-R)+A)}{T_{\mathrm{rt}}}(t-t_0)\right). \tag{3}$$

In CRDS, the decay of light circulating within the RDC is detected by monitoring the light leaking from the cavity through one of the cavity mirrors. This decay is typically digitized and fit to an exponential decay of the form

$$I(t)=I_{\mathrm{off}}+I_0\exp\left[-\frac{t}{\tau}\right] \tag{4}$$

to extract the ring-down or decay lifetime τ. In Eq. (4) I_{off} is the system offset that is usually estimated from the baseline potential before the ring-down event. The rate of this exponential decay $(1/\tau)$ is a direct measure of losses within the cavity including losses resulting from absorption by gas-phase species:

$$1/\tau=\frac{(\alpha(\lambda)L_{\mathrm{rt}}+n(1-R)+A)}{T_{\mathrm{rt}}}. \tag{5}$$

In the case where only a single absorber is present, $\alpha(\lambda)$ may be replaced by $\epsilon(\lambda)c$, where $\epsilon(\lambda)$ is the wavelength-dependent extinction coefficient of the absorbing species having concentration c. An absorption spectrum of species present within the RDC is generated by scanning the wavelength of the injected radiation while recording the decay rate.

The primary advantage of CRDS over other direct laser-absorption techniques is that the RDC decay rate is insensitive to intensity fluctuations of the laser source.[2,5,6] In theory, the only limiting noise source is the statistical fluctuation, commonly referred to as the shot noise of the photon stream exiting the cavity. Nevertheless, other noise sources routinely prevent the realization of shot-noise-limited sensitivities. A common noise source in CRDS, particularly in systems employing pulsed lasers, is that caused by excitation of multiple cavity modes. The broad linewidth of pulsed lasers typically overlaps with many longitudinal and transverse modes of the RDC. While experimentally advantageous in that every laser shot results in light coupled into the RDC, excitation of multiple cavity modes leads to mode beating within the RDC imposing noise on the detected ring-down waveform.[7] This mode beating effect has been eliminated in pulsed laser CRDS systems by employing very short cavities, whose free spectral range exceeds the laser linewidth and by carefully mode matching the laser to a single RDC mode.[8] Another method of eliminating this noise source is to employ a narrow linewidth cw laser source to allow single-mode excitation of the RDC.[9] Unlike its typical pulsed-laser system counterpart, a cw laser-based system can achieve light buildup in the RDC resulting, theoretically, in transmitted intensities approaching the intensity of the input radiation.[10] For a mode-matched cw laser system, however, achieving overlap between the cw laser source and a RDC mode becomes nontrivial because the longitudinal mode spacing of the cavity typically exceeds the laser linewidth by an order of magnitude or more. For such a system to be implemented, the laser must achieve resonance with a single RDC mode and do so repetitively as the laser wavelength is scanned throughout the desired absorption spectrum.

Recently, our group demonstrated a cavity-locked CRDS instrument that employed a frequency locking scheme developed by Drever *et al.*[11] to lock a single transverse mode (TEM_{00}) of a RDC in resonance with output of an external-cavity diode laser.[12] This system employed two orthogonal linearly polarized beams generated by a single diode laser. One beam was used to lock the laser in resonance with the RDC while the second was used to acquire ring-down decay waveforms. With this system, the frequency of the laser radiation could be continuously tuned while the laser remained locked in resonance with the TEM_{00} mode of the RDC for several minutes. This system had the added advantage that the generation of ring-down waveforms was limited only by the time required for light to buildup in the RDC so that repetition rates exceeded 30 kHz. Unfortunately, the gains afforded by this increase in the data rate could not be fully realized because of the acquisition speed of the digitizing electronics used. Furthermore, the sensitivity of the system was limited by electronic noise imposed by the detection electronics because of low cavity transmission efficiency.

This contribution describes a cw laser-locked instrument that employs a narrow linewidth Nd:YAG laser that is frequency locked to a RDC. The RDC is a three-mirror cavity with a roundtrip path length of 42 cm and mirror reflectivities of 0.99983. This reflectivity was calculated from the ring-down time by assuming that each mirror had equivalent loss. As described above, two orthogonally polarized beams generated from the same laser source are employed, but in the system reported here, both beams are used to generate servo signals that lock the laser in resonance with a single RDC mode. Cavity mirrors of modest reflectivity are used to improve cavity throughput and thereby lower the theoretical noise floor set by the shot noise of the transmitted light. The resulting cavity is also less sensitive to undesirable optical losses including scattering and absorption at the mirror surfaces. Analog detection electronics are described which eliminate noise imposed by our previous digitizing electronics, so that data acquisition speeds are in excess of 80 kHz, which allows spectral scanning speeds of 500 MHz/s.

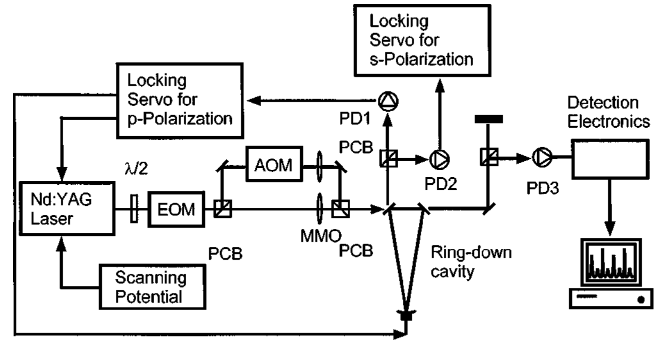

FIG. 1. Schematic diagram of laser-locked CRDS system. Abbreviations are as follows: EOM is the electro-optic modulator, $\lambda/2$ is the half-wave plate, PCB is the polarizing cube beamsplitter, AOM is the acousto-optic modulator, PD1, PD2, and PD3 are the photodetectors used to detect reflected *p*- and *s*-polarized beams and transmitted *s*-polarized light, respectively.

II. EXPERIMENT

A. Laser-locked CRDS spectrometer

Figure 1 shows a schematic diagram of the laser-locked cw-CRDS system, similar to that reported previously.[12] In this setup, the output of a Nd:YAG laser (Lightwave Electronics 122, 300 mW, tunable from 1064.44 to 1064.58 nm) is attenuated and passed through an electro-optic modulator (EOM) (New Focus 4003). The EOM places FM sidebands on the laser radiation which are used in the frequency locking scheme based on the technique developed by Drever *et al.*[11] The laser radiation is then divided into two linearly polarized beams having orthogonal polarizations using a polarizing cube beamsplitter (PCB). The beam that is *s* polarized with respect to the ring-down cavity (RDC) passes through an acousto-optic modulator (AOM) (Brimrose GPM 400-300-960) used to rapidly switch the field on and off, thereby allowing $1/\tau$ to be measured. The AOM is also used to frequency shift the *s*-polarized beam to a longitudinal mode of the RDC that is adjacent to the longitudinal mode to which the *p*-polarized radiation is locked. This procedure allows both *s*- and *p*-polarized beams to be simultaneously resonant within the three-mirror RDC. Both beams pass through mode-matching optics positioned to optimize coupling of the *s*- and *p*-polarized beams into the TEM_{00} mode of the RDC. The two beams are recombined using a PCB before being injected into the RDC.

The RDC consists of a fused silica spacer onto which three highly reflective mirrors are mounted (Research Electro-Optics).[13] Two plano–plano mirrors are attached directly to the spacer. The plano–concave mirror is mounted onto a piezoelectric transducer (PZT). The RDC roundtrip path length is 42 cm and the empty cavity ring-down lifetime is 2.8 μs. The RDC is housed in a vacuum chamber whose pressure is monitored using a capacitance manometer. The output of the RDC is detected using a photodiode (PD3) as the length of the cavity is swept through one free spectral range of the RDC. From the intensity transmitted by each transverse mode (when the cavity length is swept over a free spectral range), it was determined that over 95% of the *s*-polarized light couples into the TEM_{00} mode of the RDC. All other higher-order transverse modes of the cavity fall well outside the bandwidth of the Nd:YAG laser when the laser is locked to the TEM_{00} mode.

Light reflected by the RDC is separated into its *s*- and *p*-polarized components by a PCB and detected by two photodiodes (PD1 and PD2). The signal from each photodetector is combined with the signal used to drive the EOM using two electronic mixers. Near a cavity-laser resonance, the output of each mixer is a dc potential, or error signal, whose magnitude is proportional to the difference between the cavity resonance frequency and the frequency of the *s*- or *p*-polarized light. The error signal generated by the reflected *p*-polarized light is used by a servo to lock the laser to the RDC. This *p*-polarization locking servo consists of two actuators. High-frequency fluctuations between the laser-output frequency and the cavity-resonance frequency are fed back to the Nd:YAG laser crystal piezoelectric by an actuator having a unity gain at a frequency of 60 kHz. Low-frequency fluctuations in the *p*-polarization arm are fed back to the piezoelectric-mounted mirror of the RDC by an actuator with unity gain at a frequency of 100 Hz. The error signal generated from the reflected *s*-polarized light is used by the *s*-polarization locking servo to correct further for low-frequency fluctuations between the frequency of the *s*-polarized light and the cavity-resonance frequency. This frequency error signal is fed back to the AOM by an actuator having a unity gain at a frequency of 100 Hz. With both *s*- and *p*-polarization servos in operation, high-speed scans (500 MHz/s) were obtained by scanning the wavelength of the laser. The laser remains locked to the RDC for hours with both servos in operation.

The *s*-polarized light exiting the cavity is separated from the transmitted *p*-polarized light using a PCB and detected using a photodiode (PD3). The signal generated by PD3 is detected using the analog detection scheme described in Sec. II C. For comparison, it can also be digitized using a digitizing oscilloscope (Hewlett-Packard HP51540, LeCroy 1040, or Gage 6012Gagescope). In the latter procedure, digitized waveforms are numerically fitted on a personal computer with a weighted Levenberg–Marquardt algorithm to extract the decay rate.

B. Photodetection spectral-noise density

The three photodetectors (PD1, PD2, and PD3) were constructed from commercially available components and are shown schematically in Fig. 2(a). Each detector consists of an InGaAs photodiode that is reverse biased and amplified using two low-noise amplification stages. The output voltage

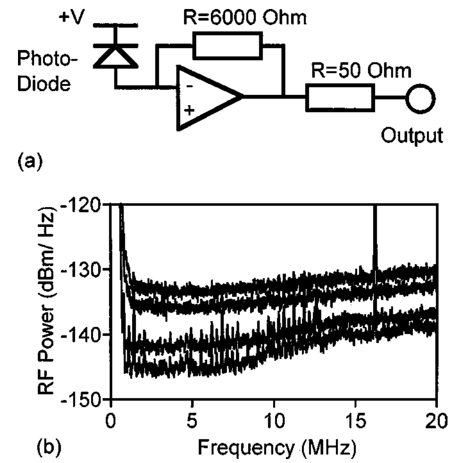

FIG. 2. (a) Schematic diagram of detector amplifier electronics; (b) spectral-noise density of photodetector with different light levels incident on the photodetector.

V_a of a photodetector is a function of the incident optical power P_0 and is given by

$$V_a \pm \Delta V_a = P_0 \Re R_f \pm \sqrt{(2eP_0 \Re R_f \pm \Delta v_e^2)B}, \tag{6}$$

where $\Re$ is the photodetector's responsivity (0.77 A/W at 1064 nm for the diode used), $R_f = 6000\,\Omega$ is the photodetector's transimpedance, e is the electronic charge, ΔV_a is the voltage noise from the photon-induced shot noise, and Δv_e is the amplifier voltage noise, which is measured with a resolution bandwidth B. The spectral-noise density at the output of the photodetector was measured on a rf spectrum analyzer (SA) (HP8590L).

Figure 2(b) shows the spectral-noise density for three operating photocurrents on a dBm scale (decibel above 1 mW of rf power) normalized to a 1 Hz measurement resolution bandwidth, and measured from near dc to 20 MHz. These three photocurrents were used in the following experiments.

In Fig. 2(b), trace (a) is the spectral-noise density of the photodetector under the condition in which no laser light is incident on the detector, otherwise known as the photodetector electronic noise floor. Traces (b), (c), and (d) show the spectral-noise density when sufficient laser radiation is incident on the photodetector to produce 0.4, 3.33, and 6 V of signal, respectively. Note that all three laser light levels were sufficient to generate observable photon-induced shot noise.

The noise performance of this photodetector system is summarized in Table I. The noise powers were measured at 5 MHz because the noise level from near dc to 5 MHz was approximately constant. Table I lists:

(i) the conversion from the total rf SA noise power (in dBm/$\sqrt{\text{Hz}}$) to rf power in W using the relation

$$x\ \text{dBm} = 10\log_{10}(\text{rf power (W)}/10^{-3}\text{(W)}), \tag{7}$$

where x is the stated noise value, and the rf power is measured through the 50 Ω input impedance of the SA;

(ii) the conversion from total rf power (which is shot noise power plus electronic noise power) to shot noise rf power;

TABLE I. Summary of the noise spectral densities, and signal-to-noise calculations and measurements shown in Fig. 2.

Trace	(a)	(b)	(c)	(d)
Noise power at 5 MHz(dBm/$\sqrt{\text{Hz}}$)	−145.3	−144.8	−135.8	−133.8
Total rf noise powder (W) due from shot noise +electronic noise	3.68×10^{-18}	6.65×10^{-18}	2.65×10^{-17}	4.20×10^{-17}
rf noise powder (W) due to shot noise		3.68×10^{-18}	2.35×10^{-17}	3.90×10^{-17}
Voltage noise (V) at input of SA due to shot noise for a 50 Ω output resistance of PD and 50 Ω input resistance of SA		1.92×10^{-8}	4.85×10^{-8}	6.24×10^{-8}
Current noise (A) at PD needed to generate noise level at SA for a transimpedance of 6000 A/V		3.20×10^{-12}	8.08×10^{-12}	1.04×10^{-11}
dc current (A) at PD assuming a transimpedance of 6000 A/V		6.67×10^{-5}	5.5×10^{-4}	1×10^{-3}
Theoretical shot noise current (A)		4.62×10^{-12}	1.33×10^{-11}	1.79×10^{-11}
Signal-to-noise ratio		2.1×10^{7}	6.8×10^{7}	9.6×10^{7}

(iii) the conversion from noise power to noise voltage using the relation

$$V_{\text{noise}}=\sqrt{P_{\text{noise}}R}, \tag{8}$$

where R is the total load resistance arising from the output amplification stage and the input SA stage;

(iv) the conversion from voltage noise to current noise at the photodetector obtained by dividing the noise voltage by R_f, and

(v) the dc photocurrent that generates the three noise levels, and the theoretical shot-noise current associated with these levels calculated using the relationship

$$\frac{\Delta i_{\text{shot}}}{\sqrt{\text{Hz}}}=\sqrt{2ei_{\text{dc}}}, \tag{9}$$

where Δi_{shot} is the noise current and i_{dc} is the dc photocurrent. The calculated and measured noise currents agree to within a factor of approximately 0.6.

The computed signal-to-noise ratio (S/N) for this system ranges from 2.1×10^{7} for the low light level to 9.6×10^{7} for the high light level. Observation simultaneously of the dc and the noise components with a 1 Hz resolution bandwidth would require at least a 27-bit digitizer to fully exploit the S/N levels of the system.

C. Analog detection scheme

The analog detection system is depicted schematically in Fig. 3(a), while traces showing three ring-up and ring-down cycles at four different points within the detection system are shown in Fig. 3(b). In this scheme, the output of PD3 is logarithmically amplified to convert the exponentially decaying potential to a linearly decaying potential. The output of the logarithmic amplifier is then differentiated by an analog differentiating circuit. The dc potential generated by the differentiator over the decay period is proportional to $1/\tau$. An automatic-gain-control amplifier (AGC) gates the output of the differentiator to eliminate the ring-up portion of the waveform. In other words, the AGC multiplies the output of the differentiator by zero during the unwanted portion of the waveform. A home-built pulse-delay generator triggered by the same signal was used to switch the *s*-polarized light gates to AGC. During spectral scanning, the switching speed of the system is set to 80 kHz, which corresponds to the light being on or off for 6.25 μs intervals. The AGC preserves approximately 5 μs of the ring-down signal. To measure small changes in the potential generated by the differentiator during the ring-down event, the nonzero output of the AGC is summed with an offset voltage to bring the potential close to zero and is amplified using a low-noise amplifier. This amplified signal is measured by a lock-in amplifier with an integration period of 100 ms. Finally, the analog output of the lock-in and the potential used to scan the wavelength of the Nd:YAG laser are recorded simultaneously using a digital oscilloscope.

III. RESULTS AND DISCUSSION

A. Digital data acquisition

Initially, digitizing electronics were used to acquire ring-down decay waveforms and a weighted fit was performed to extract the decay rate $(1/\tau)$. Two deficiencies in this digital-acquisition system, however, prompted us to investigate

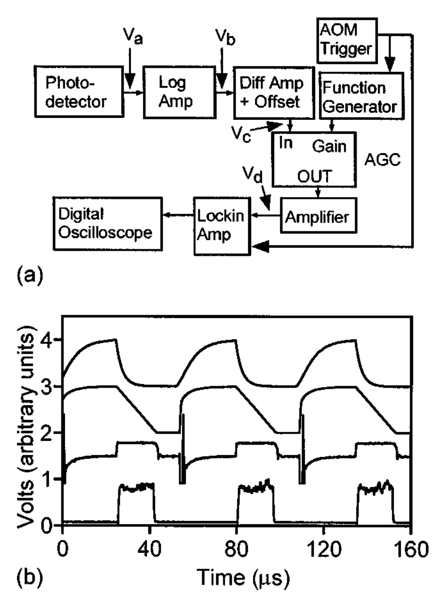

FIG. 3. (a) Schematic diagram of analog detection system; (b) traces obtained at various points within the analog detection system.

other methods of detection. First, it is evident that the data acquisition speed for a commercial digitizing oscilloscope limits the overall speed of the laser-locked CRDS instrument. Using the digitizer with the fastest data-transfer rate to the fitting PC (6012Gagescope), ring-down waveform acquisition and fit rates are limited to approximately 600 Hz. While acquisition rates of 200 Hz have been achieved with other schemes,[14] these rates falls well short of the 80 kHz set by the optical system.

Second, the digitizing electronics imposes a limitation caused by the noise of the digitizer. As noted above, a digitizer with at least 27-bit resolution is required to achieve shot-noise-limited sensitivity at the beginning of the waveform if a 1 Hz resolution bandwidth is needed. Experimentally, however, we have found that commercial digitizing oscilloscopes, which have between 8- and 12-bits of vertical resolution, impose additive electronic noise that far exceeds that imposed by the digitization process for typical microsecond ring-down waveforms. In the Appendix we present a detailed consideration of the problems associated with the use of digitizers in the analysis of cavity ring-down waveforms. These two problems motivated us to seek to develop analog detection electronics that avoid the limitations imposed by commercially available digitizing oscilloscopes.

B. Analog detection scheme

Figure 3(a) shows a schematic of the analog electronics that follow PD3. In this section we derive the signal and noise transfer during the ring-down process. The reduction of signal strength during the ring-down process is given by

$$V_a(t)\pm\Delta V_a(t)=P_0\Re R_f\exp\left(-\frac{t}{\tau}\right)\pm\sqrt{\left[2eP_0\Re R_f\exp\left(-\frac{t}{\tau}\right)\pm\Delta v_e^2\right]B}. \quad (10)$$

The photodetector signal is conditioned by a logarithmic amplifier[15] to produce a linearized signal;

$$V_b(t)\pm\Delta V_b(t)=k\log_{10}[V_a(t)\pm\Delta V_a(t)], \quad (11)$$

where k is a constant of proportionality and has units V.

In our experiment, the signal-to-noise ratio is always large ($>10^5$). Hence we can approximate that the output voltage after the log-amp to be[16]

$$V_b(t)\pm\Delta V_b(t)\approx k\ln\left[P_0\Re R_f\exp\left(-\frac{t}{\tau}\right)\right]\pm k\frac{\sqrt{\left[2eP_0\Re R_f\exp\left(-\frac{t}{\tau}\right)\pm\Delta v_e^2\right]B}}{P_0\Re R_f\exp\left(-\frac{t}{\tau}\right)}, \quad (12)$$

which expands to

$$V_b(t)\pm\Delta V_b(t)=-\frac{kt}{\tau}+k\ln(P_0\Re R_f)\pm k\frac{\sqrt{\left[2eP_0\Re R_f\exp\left(-\frac{t}{\tau}\right)\pm\Delta v_e^2\right]B}}{P_0\Re R_f\exp\left(-\frac{t}{\tau}\right)}. \quad (13)$$

It is clear from Eq. (13) that the S/N after the log-amp is greater than the input S/N by the factor $\ln[P_0\Re R_f\times\exp(-t/\tau)]$.

The log-amp voltage is then differentiated by an appropriate amplifier to give the output voltage:

$$V_c(t)\pm\Delta V_c(t)=\frac{d}{dt}[V_b(t)\pm\Delta V_b(t)], \quad (14)$$

which simplifies to

$$V_c(t)\pm\Delta V_c(t)=-\frac{G(\omega_{\rm rd})k}{\tau}\times\frac{G(\omega_{\rm chop})k\sqrt{\left[2eP_0\Re R_f\exp\left(-\frac{t}{\tau}\right)\pm\Delta v_e^2\right]B}}{P_0\Re R_f\exp\left(-\frac{t}{\tau}\right)}, \quad (15)$$

where $G(\omega_{\rm rd})$ and $G(\omega_{\rm chop})$ are gain constants for the signal and the noise components. $G(\omega_{\rm rd})$ has units of s, whereas $G(\omega_{\rm chop})$ is unitless. $G(\omega_{\rm rd})$ was measured using a test input triangle wave to have the value 0.25 μs, and $G(\omega_{\rm chop})$ was measured using a test sine wave to have the value 0.12 at the chopping frequency.

Finally, the magnitude of the differentiated signal is compared to a reference signal at the experimental chopping frequency by a lock-in amplifier. The S/N is thus given by

$$\mathrm{S/N}\approx\frac{0.7P_0\Re R_f\exp\left(-\frac{t}{\tau}\right)}{\sqrt{\left[2eP_0\Re R_f\exp\left(-\frac{t}{\tau}\right)\pm\Delta v_e^2\right]B}}. \quad (16)$$

Hence, the S/N at the output of the differentiator stage is smaller by 0.7 times the S/N at the output of the photodetector. Note, that we assumed that the noise measurement is made at a fixed time t.

C. Performance of laser-locked CRDS instrument

Figure 4 shows an absorption spectrum of CO_2 from 9393.91 to 9394.04 cm^{-1} obtained using the laser-locked CRDS instrument described above with the analog detection circuit. The feature in this spectrum is attributed to the R(8) line of the CO_2 $(0,0^0,0)-(2,0^0,3)$ band. The traces shown were obtained with 3.0, 2.0, and 1.0 Torr of CO_2 in the vacuum chamber containing the RDC. Each trace represents a single scan with a lock-in amplifier integration period of

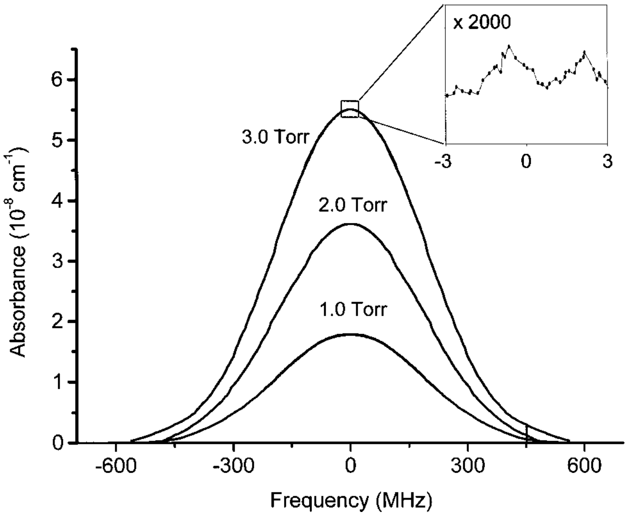

FIG. 4. Absorption spectra of CO_2 obtained at 3.0, 2.0, and 1.0 Torr using the CRDS system and analog detection system described here. Noise on the scan obtained at 3.0 Torr is shown on an expanded scale.

100 ms and required 8 s to acquire. The spectral resolution of each scan is set by the linewidth of the RDC at 75 kHz. Scans were obtained with 25 mW of *s*-polarized light incident on the RDC of which 2.6 mW was transmitted by the RDC and incident on PD3 at the beginning of each ring-down waveform. A portion of the scan obtained at 3 Torr is shown in expanded scale to show the noise on the scan. The background noise floor for this system is within the limit imposed by the lock-in amplifier's dynamic range (100 dB) but is again limited by the final digitization electronics (our 12-bit digitizer has only 60 dB of dynamic range). That is, the noise measured is approximately 60 dB lower than the signal strength. Given the background noise observed for each of the three scans, the minimum detectable absorption limit[3] (MDAL) for this system calculated at the peak of the absorption profile is $8.8\times 10^{-12}\,\mathrm{cm}^{-1}\,\mathrm{Hz}^{-1/2}$. The MDAL was also determined from these scans by comparing the integrated noise of a baseline scan obtained over the same spectral region with the integrated intensity of the absorption feature. Using this method a MDAL of $1.0\times 10^{-12}\,\mathrm{cm}^{-1}\,\mathrm{Hz}^{-1/2}$ was calculated.

While the stability of the system over short time periods (10–15 s) allowed such high sensitivities to be obtained, fluctuations in the measured signal over longer timescales degraded the performance of the system. Figure 5 shows a plot obtained by setting the frequency of the laser output on the peak of the absorption feature and measuring changes in

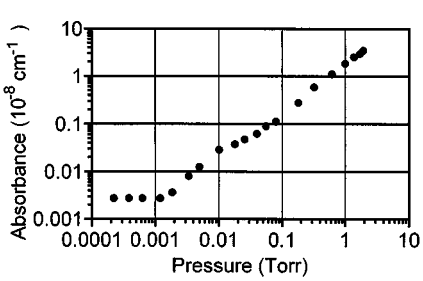

FIG. 5. Observed absorbance loss plotted as a function of CO_2 pressure with the laser frequency set at the peak of the CO_2 absorption feature.

the output of the lock-in amplifier as the vacuum chamber was slowly evacuated. Each scan was obtained over approximately 5 min and error bars represent the standard deviation in 20 points obtained over 2 s. We see that the intensity of the peak decays linearly from 2 Torr down to a minimum detectable pressure of approximately 0.005 Torr. This detection sensitivity corresponds to a MDAL of $8.8\times 10^{-12}\,\mathrm{cm}^{-1}\,\mathrm{Hz}^{-1/2}$.

We can compare this result with the MDAL that could be obtained from a shot-noise-limited direct absorption experiment of the same effective path length (assuming that the measurement was possible) using the relationship[17]

$$\mathrm{MDAL}=\sqrt{\frac{2e}{P_0\Re R_f}}\frac{1}{L_{\mathrm{eff}}}, \tag{17}$$

where

$$L_{\mathrm{eff}}=(2L_{\mathrm{rt}}F/\pi), \tag{18}$$

L_{rt} is the roundtrip path length, and F is the cavity finesse, which is related to the mirror reflectivity, R, by

$$F=\frac{2\pi}{\delta_c}\approx\frac{2\pi}{n(1-R)+A}. \tag{19}$$

Hence, the MDAL value for 3.33 V from the photodetector, corresponding trace (c) of Fig. 2(b), would be $9.2\times 10^{-14}\,\mathrm{cm}^{-1}\,\mathrm{Hz}^{-1/2}$. Therefore, this CRDS spectrometer is less than two orders of magnitude in sensitivity away from this fundamental limit.

IV. DISCUSSION

The results from this laser-locked cavity ring-down spectrometer demonstrate that ultrasensitive absorption measurements are possible with a CRDS system employing a cw-laser source and analog detection system. The analog detection system described here permits acquisition and analysis in real time of the RDC decay time constant. This system allows full realization of the improved repetition rates afforded by CRDS instruments using cw lasers. It also eliminates noise imposed on ring-down decay waveforms by commercial digitizing oscilloscopes. by striving toward shot-noise-limited detection of decay waveforms generated by lower finesse RDCs, we have achieved sensitivities that exceed those obtained with cavities having significantly longer roundtrip path lengths and higher finesse. With continued development, we believe that CRDS will become a tool for ultrasensitive measurements whenever absorption spectroscopy can be employed to advantage.

ACKNOWLEDGMENTS

We thank J.L. Hall and M.D. Levenson for useful discussions. Support is gratefully acknowledged from the Air Force Office of Scientific Research under Contract No. F49620-97-1-0316, and the Department of Energy under Contract No. DE-FG 03-92-ER14304-A006.

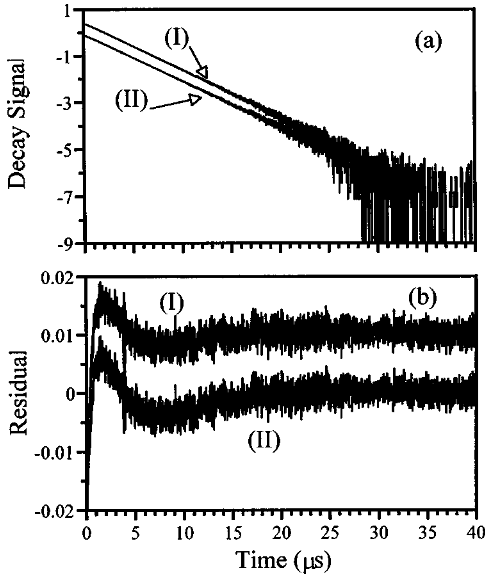

FIG. 6. Ring-down decay trace obtained using digitizing oscilloscope and fit residuals obtained by fitting decays generated by the CRDS system described here and a simple RC circuit.

APPENDIX: NOISE INTRODUCED BY DIGITIZATION OF CAVITY RING-DOWN WAVEFORMS

Figure 6(a) shows a typical ring-down waveform generated by the laser-locked instrument described above (curve I), and a decay signal generated by an electronic RC network (curve II). Note that we are considering systems that have a time constant of 3 μs or less. Figure 6(b) presents the residuals obtained after performing a weighted fit of the ring-down waveform to the equation $I=I_0\exp(-t/\tau)$ for curve I and curve II. Identical residuals are observed using three different oscilloscopes in combination with two different photodetectors. The fact that the residuals observed for the RC circuit and the ring-down decay resemble one another indicates that the digitizers employed here inherently impart electronic noise onto the exponentially decaying signal. This noise ultimately limits the error in the determination of the ring-down rate for a single decay waveform.

The residuals arise from imperfect relative accuracy and differential nonlinearity (DNL) of the analog-to-digital converter (ADC) and other data acquisition circuitry in the oscilloscopes.[18] The error in the digitized voltage is measured in units of what is called the least significant bit (LSB). For all the oscilloscopes used in these experiments, the DNL did not exceed 1 LSB. Hence, DNL is not the primary limiting digitizer noise.

Relative accuracy is a measure (in LSB) of the worst-case deviation from a linearly changing voltage. The relative accuracy is determined by sweeping an applied voltage from the negative to the positive full-scale reading and digitizing it. Figure 7(a) shows the relative accuracy of an 8-bit HP oscilloscope compared to an ideal digitized linear decay. Figure 7(b) shows the residual for a 12-bit Gagescope6012 oscilloscope. These results show that the relative accuracy is significantly worse than one bit. Good relative accuracy is important in that it ensures that the translation from the actual voltage value to the binary code of the ADC is accurate.

In typical CRDS experiments in which the detector noise exceeds the relative error, the quality of the exponential fit can be improved by acquiring many points for a single decay waveform. An increase in the number of points acquired, however, slows down the data acquisition rate. Moreover, for signals whose S/N exceeds the digitizer bit-number, the relative error has proven to be the primary limiting factor in the smallest sensitivity achievable. The relative error directly limits the measurement of a single-shot ring-down rate. It is clear that the noise imposed by the digitizing oscilloscope prevents realization of even digitization-limited ring-down rates. This limitation for ring-down decay waveforms with time constants of only a few microseconds prompted us to develop analog detection electronics that avoid noise imposed by commercially available digitizing oscilloscopes.

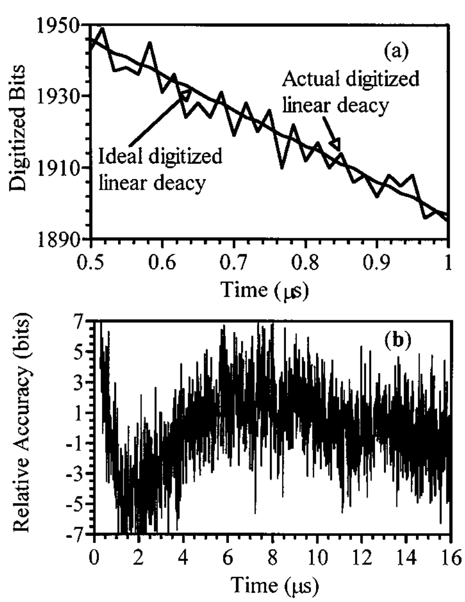

FIG. 7. (a) Digital nonlinearity and (b) relative accuracy normalized to bits, for a typical 12-bit digitizing oscilloscope.

[1] A. O'Keefe and D. A. G. Deacon, Rev. Sci. Instrum. **59**, 2544 (1988).
[2] P. Zalicki and R. N. Zare, J. Chem. Phys. **102**, 2708 (1995).
[3] *ACS Symposium Series*, edited by K. W. Busch and M. A. Busch (American Chemical Society, Washington, DC, 1999), Vol. 720 (complete volume).
[4] A. E. Siegman, *Lasers* (University Science Books, Mill Valley, CA, 1986).
[5] K. K. Lehmann and D. Romanini, J. Chem. Phys. **105**, 10263 (1996).
[6] J. T. Hodges, J. P. Looney, and R. D. van Zee, J. Chem. Phys. **105**, 10278 (1996).
[7] J. Martin *et al.*, Chem. Phys. Lett. **28**, 63 (1996).
[8] R. D. van Zee, J. T. Hodges, and J. P. Looney, Appl. Opt. **38**, 3951 (1999).
[9] K. K. Lehmann, U.S. Patent No. 5,528,04 (1996).
[10] E. R. Crosson *et al.*, Rev. Sci. Instrum. **70**, 4 (1998).
[11] R. W. P. Drever *et al.*, Appl. Phys. B: Photophys. Laser Chem. **31**, 97 (1983).
[12] B. A. Paldus *et al.*, J. Appl. Phys. **83**, 3991 (1998).
[13] A. Ueda *et al.*, Opt. Rev. **3**, 369 (1996).
[14] D. Romanini *et al.*, Chem. Phys. Lett. **264**, 316 (1997).
[15] P. Horowitz and W. Hill, *The Art of Electronics* (Cambridge University Press, Cambridge, 1996).
[16] C. Hau, Proc. IEEE **57**, 1667 (1969).
[17] J. Ye, L.-S. Ma, and J. L. Hall, J. Opt. Soc. Am. B **15**, 6 (1998).
[18] Data Acquisition Tutorial, National Instruments Catalogue, 1998, p. 190.